presence, extent, and vulnerable characteristics of NCPs, as assessed by 64-slice CTA. Our findings support the notion that the accumulation of VAT may contribute to the progression and instability of coronary atherosclerotic plaques. Studies of the long-term cardiovascular event risk in patients with visceral adiposity are important, and 64-slice CTA may offer an approach to improve risk stratification in such patients.

References

1. Manson JE, Colditz GA, Stampfer MJ, et al. A prospective study of obesity and risk of coronary heart disease in women. N Engl J Med 1990;322:882-9.
2. Kissebah AH, Vydelingum N, Murray R, et al. Relation of body fat distribution to metabolic complications of obesity. J Clin Endocrinol Metab 1982;54:254-60.
3. Després JP, Moorjani S, Lupien PJ, Tremblay A, Nadeau A, Bouchard C. Regional distribution of body fat, plasma lipoproteins, and cardiovascular disease. Arteriosclerosis 1990;10:497-511.
4. Yusuf S, Hawken S, Ounpuu S, et al. Obesity and the risk of myocardial infarction in 27,000 participants from 52 countries: a case-control study. Lancet 2005;366:1640–9.
5. Nicklas BJ, Penninx BW, Cesari M, et al. Association of visceral adipose tissue with incident myocardial infarction in older men and women: the Health, Aging and Body Composition Study. Am J Epidemiol 2004;160:741-9.
6. Ohashi N, Yamamoto H, Horiguchi J, et al. Visceral fat accumulation as a predictor of coronary artery calcium as assessed by multislice computed tomography in Japanese patients. Atherosclerosis 2009;202:192–9.
7. Yamagishi M, Terashima M, Awano K, et al. Morphology of vulnerable coronary plaque: insights from follow-up of patients examined by intravascular ultrasound before an acute coronary syndrome. J Am Coll Cardiol 2000;35:106-11.
8. Varnava AM, Mills PG, Davies MJ. Relationship between coronary artery remodeling and plaque vulnerability. Circulation 2002;105:939-43.
9. Motoyama S, Kondo T, Sarai M, et al. Multislice computed tomographic characteristics of coronary lesions in acute coronary syndromes. J Am Coll Cardiol 2007;50:319–26.
10. Ehara S, Kobayashi Y, Yoshiyama M, et al. Spotty calcification typifies the culprit plaque in patients with acute myocardial infarction: an intravascular ultrasound study. Circulation 2004;110:3424-9.
11. Leber AW, Becker A, Knez A, et al. Accuracy of 64-slice computed tomography to classify and quantify plaque volumes in the proximal coronary system: a comparative study using intravascular ultrasound. J Am Coll Cardiol 2006;47:672–7.

12. Kitagawa T, Yamamoto H, Ohhashi N, et al. Comprehensive evaluation of non-calcified coronary plaque characteristics detected using 64-slice computed tomography in patients with proven or suspected coronary artery disease. Am Heart J 2007;154:1191–98.
13. Kitagawa T, Yamamoto H, Horiguchi J, et al. Characterization of noncalcified coronary plaques and identification of culprit lesions in patients with acute coronary syndrome by 64-slice computed tomography. JACC Cardiovasc Imaging 2009;2:153–60.
14. Teramoto T, Sasaki J, Ueshima H, et al. Executive Summary of Japan Atherosclerosis Society (JAS) Guideline for Diagnosis and Prevention of Atherosclerotic Cardiovascular Diseases for Japanese. J Atheroscler Thromb 2007;14:45-50.
15. Kajinami K, Seki H, Takekoshi N, Mabuchi H. Coronary calcification and coronary atherosclerosis: site by site comparative morphologic study of electron beam computed tomography and coronary angiography. J Am Coll Cardiol 1997;29:1549-56.
16. Budoff MJ, Shaw LJ, Liu ST, et al. Long-term prognosis associated with coronary calcification: observations from a registry of 25,253 patients. J Am Coll Cardiol 2007;49:1860–70.
17. Pundziute G, Schuijf JD, Jukema JW, et al. Prognostic value of multislice computed tomography coronary angiography in patients with known or suspected coronary artery disease. J Am Coll Cardiol 2007;49:62–70.
18. Lamarche B, Tchernof A, Mauriège P, et al. Fasting insulin and apolipoprotein B levels and low-density lipoprotein particle size as risk factors for ischemic heart disease. JAMA 1998;279:1955–61.
19. Seidell JC, Cigolini M, Deslypere JP, Charzewska J, Ellsinger BM, Cruz A. Body fat distribution in relation to physical activity and smoking habits in 38-year-old European men. The European Fat Distribution Study. Am J Epidemiol 1991;133:257-65.
20. Fantuzzi G, Mazzone T. Adipose tissue and atherosclerosis: exploring the connection. Arterioscler Thromb Vasc Biol 2007;27:996–1003.
21. Kappert K, Meyborg H, Clemenz M, et al. Insulin facilitates monocyte migration: a possible link to tissue inflammation in insulin-resistance. Biochem Biophys Res Commun 2008;365:503–8.
22. Hajer GR, van Haeften TW, Visseren FL. Adipose tissue dysfunction in obesity, diabetes, and vascular diseases. Eur Heart J 2008;29:2959–71.
23. Bluemke DA, Achenbach S, Budoff M, et al. Noninvasive coronary artery imaging: magnetic resonance angiography and multidetector computed tomography angiography: a scientific statement from the American Heart Association Committee on cardiovascular imaging and intervention of the council on

cardiovascular radiology and intervention, and the Councils on Clinical Cardiology and cardiovascular disease in the young. Circulation 2008;118:586–606.

Figure legends

Figure 1 Coronary CT Angiography in a 74-Year-Old Man with High VAT Presenting with Unstable Angina Pectoris

Panel A shows a significant stenotic lesion in the proximal left anterior descending artery (arrowhead). The stretched multiplanar reconstruction image of the vessel shows obstructive NCP with positive remodeling and adjacent spotty calcium (Panel B, arrow). The cross-sectional vessel areas of the reference site (a) and lesion (b) are 26 and 32 mm^2, respectively. Therefore, the remodeling index is 1.23. The minimum CT density of the lesion is 21 HU (b). The small circles within the outer vessel boundaries indicate regions of interest (area = 1 mm^2) (a, b). Adjacent spotty calcium is observed in the cross-sectional image (c). Panel C shows the abdominal adipose tissue areas at the level of the umbilicus. Regions of blue and red color indicate visceral (162 cm^2) and subcutaneous (151 cm^2) adipose tissue areas, respectively. CT = computed tomography; NCP = noncalcified coronary plaque; VAT = visceral adipose tissue.

Figure 2 Prevalence of NCP Characteristics in Patients with High and Low VAT

High VAT indicates VAT area above the sex-specific median value (men 126 cm^2, women 91 cm^2) and low VAT is below the median. Open and solid bars indicate low and high VAT, respectively. PR = positive remodeling; other abbreviations as in Figure 1. †, $p < 0.01$; *, $p < 0.05$.

Figure 3 Comparison of CAC Score and the Number of NCPs Between Patients with High and Low VAT area

The higher VAT groups had significantly higher median levels of CAC scores and more NCPs in both sexes. *Boxes*, 25th and 75th percentiles; *lines*, 5th and 95th percentiles for the data (left panel). The number of NCPs is shown as the mean ± SE. (right panel). CAC = coronary artery calcium; other abbreviations as in Figure 2.

Table 1 Characteristics of the Study Patients with High and Low VAT area

	Men (n = 267)		Women (n = 160)	
	High VAT (n = 133)	Low VAT (n = 134)	High VAT (n = 80)	Low VAT (n = 80)
Age (yrs)	65 ± 10	64 ± 12	71 ± 10	68 ± 11
BMI (kg/m^2)	25.7 ± 2.7†	22.4 ± 3.1	24.7 ± 3.4†	22.1 ± 3.4
WC (cm)	95.8 ± 7.5†	84.7 ± 7.6	93.7 ± 7.7†	82.3 ± 8.4
SAT (cm^2)	143 ± 53†	99 ± 46	190 ± 71†	141 ± 61
Hypertension, n (%)	92 (69)*	76 (57)	48 (60)*	35 (44)
Hypercholesterolemia, n (%)	80 (60)*	61 (46)	48 (60)*	32 (40)
Diabetes mellitus, n (%)	79 (59)†	50 (37)	41 (51)†	23 (29)
Current smoking, n (%)	73 (55)	66 (49)	13 (16)	6 (8)
Total cholesterol (mg/dl)	201 ± 34	196 ± 41	203 ± 39	204 ± 51
Triglycerides (mg/dl)	156 (109–231)†	111 (83–157)	146 (110–210)†	98 (75–133)
HDL cholesterol (mg/dl)	48 ± 14†	59 ± 18	57 ± 16†	68 ± 17
LDL cholesterol (mg/dl)	119 ± 29	114 ± 32	119 ± 35	119 ± 47
HbA1c (%)	6.3 ± 1.3†	5.8 ± 1.3	6.3 ± 1.2†	5.8 ± 1.2
Medications				
Antihypertensive agents, n (%)	49 (37)*	32 (24)	20 (25)	22 (28)
Lipid-lowering agents, n (%)	39 (29)	32 (24)	22 (28)	18 (23)
Hypoglycemic agents, n (%)	43 (32)*	27 (20)	28 (35)*	15 (19)

High VAT indicates VAT area above the sex-specific median value (men 126 cm^2, women 91 cm^2) and low VAT indicates VAT area below the median value. Values are expressed as number (percent), means ± SD or medians (interquartile range). BMI = body mass index; HbA1c = hemoglobin A1c; HDL = high-density lipoprotein; LDL = low-density lipoprotein; SAT = subcutaneous adipose tissue; VAT = visceral adipose tissue; WC = waist circumference. *, $p < 0.05$; †, $p < 0.01$.

	Presence				Extent			
	Univariate		Multivariate		Univariate		Multivariate	
	OR (95% CI)[a]	p-value	OR (95% CI)[a]	p-value	β[b]	p-value	β[b]	p-va
(per 11 yrs)	1.21 (1.00–1.47)	0.05	1.42 (1.10–1.84)	0.007	0.11	0.08	0.13	0.0
men)	3.04 (2.02–4.59)	<0.0001	1.58 (0.85–2.95)	0.15	0.32	<0.0001	0.15	0.0
(per 3.5 kg/m^2)	1.13 (0.94–1.37)	0.21	0.70 (0.48–1.02)	0.07	0.07	0.31	-0.11	0.3
(per 9.6 cm)	1.37 (1.13–1.69)	0.0016	1.48 (0.87–2.59)	0.16	0.15	0.03	-0.08	0.5
(per 58 cm^2)	2.13 (1.71–2.82)	<0.0001	1.79 (1.22–2.77)	0.004	0.39	<0.0001	0.34	0.0
(per 65 cm^2)	0.82 (0.67–1.00)	0.043	0.68 (0.43–1.05)	0.09	-0.12	0.07	-0.05	0.6
rtension	2.18 (1.46–3.25)	0.0001	1.61 (0.94–2.78)	0.08	0.31	<0.0001	0.19	0.0
rcholesterolemia	2.35 (1.59–3.52)	<0.0001	2.24 (1.31–3.88)	0.004	0.29	<0.0001	0.23	0.0
etes mellitus	2.03 (1.36–3.04)	0.0005	2.00 (1.06–3.84)	0.03	0.28	<0.0001	0.18	0.0

Table 2 Association of VAT with the Presence and Extent of NCP

nt smoking	2.93 (1.91–4.57)	<0.0001	2.12 (1.25–3.63)	0.006	0.32	<0.0001	0.18	0.0
ypertensive agents	1.22 (0.79–1.89)	0.37	0.70 (0.39–1.26)	0.24	0.12	0.11	-0.05	0.5
l-lowering agents	1.74 (1.10–2.79)	0.02	1.08 (0.58–2.03)	0.80	0.16	0.04	-0.03	0.7
glycemic agents	1.53 (0.98–2.43)	0.07	0.63 (0.30–1.30)	0.22	0.25	0.001	0.01	0.8

[a] Odds ratio (95% confidence interval) for the presence of NCP associated with the presence of covariates in dichotomous variables or a 1-SD increase in continuous variables. [b] β indicates beta-estimate, predicted increase in the number of detectable NCPs. NCP = noncalcified coronary plaque; other abbreviations as in Table 1.

Table 3 Relationship Between VAT and the Presence of NCP with Vulnerable Characteristics

	Age- and sex-adjusted		Multivariate[b]	
	OR (95% CI)[a]	p-value	OR (95% CI)[a]	p-value
Positive remodeling	2.0 (1.57–2.57)	<0.0001	1.69 (1.16–2.51)	0.007
Low CT density	1.66 (1.33–2.11)	<0.0001	1.57 (1.08–2.32)	0.02
Spotty calcium	1.69 (1.34–2.17)	<0.0001	1.53 (1.03–2.31)	0.04
All three characteristics	1.89 (1.47–2.54)	<0.0001	1.71 (1.09–2.72)	0.02

[a] Odds ratio (95% confidence interval) for the presence of each vulnerable NCP characteristic per 1-SD (58 cm^2) increase in VAT. [b] Adjusted for age, sex, BMI, SAT, WC, hypertension, hypercholesterolemia, diabetes mellitus, current smoking, and medication usage. CT = computed tomography; NCP = noncalcified coronary plaque; other abbreviations as in Table 1.

Figure 1

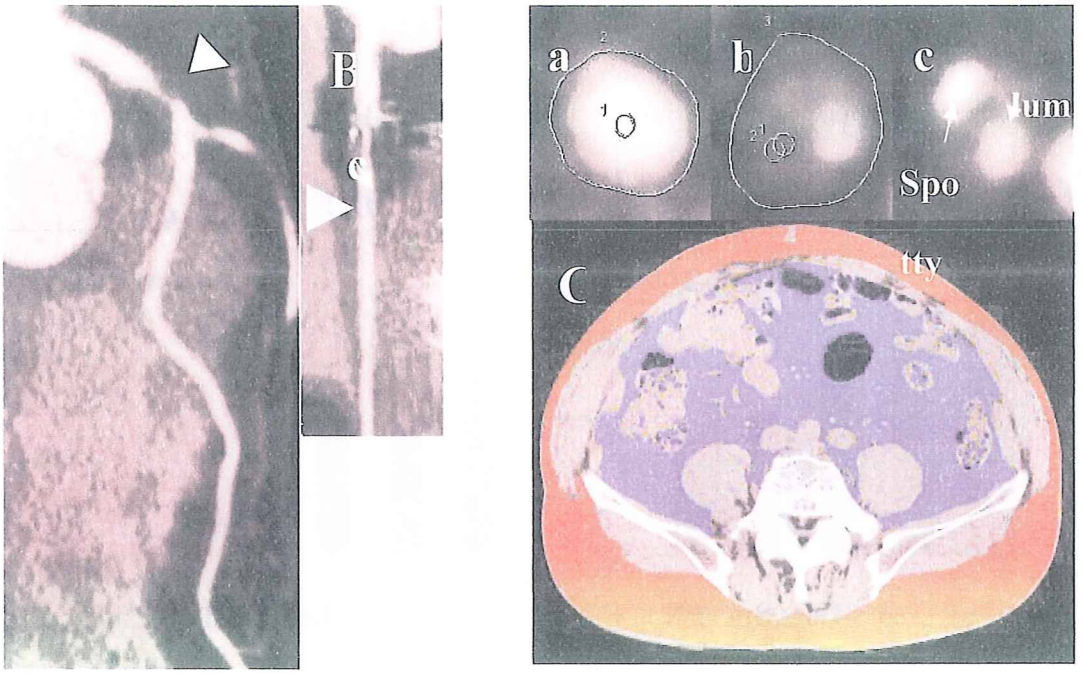

Figure 2

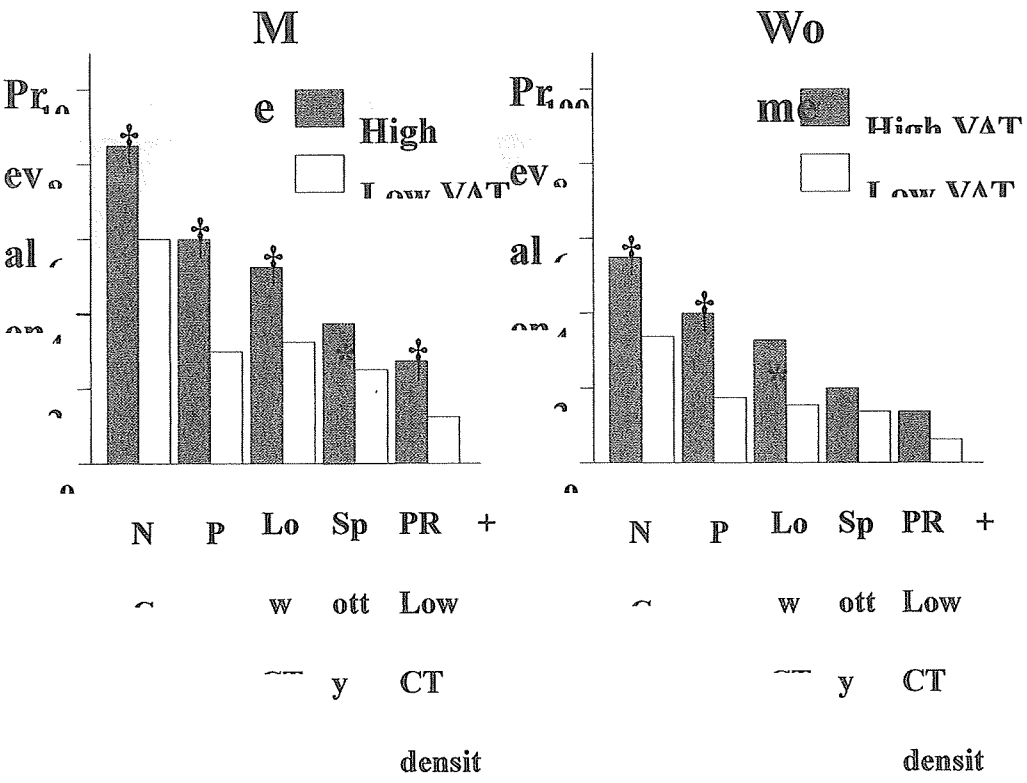
M
e
High
Low VAT
Wo
me
High VAT
Low VAT
N
P
Lo
w
Sp
ott
y
PR
+
Low
CT
densit

Evaluation of Attenuation-Based Tube Current Control in Coronary Artery Calcium Scoring on Prospective ECG-triggered 64-detector CT[1]

Jun Horiguchi, MD, Noriaki Matsuura, MD, Hideya Yamamoto, MD, Toshiro Kitagawa, MD, Kenichi Sato, PhD, Yasuki Kihara, MD, Katsuhide Ito, MD

Rationale and Objectives. The aims of this study were to investigate image noise (standard deviation of computed tomographic value) and to assess variability in repeated coronary artery calcium (CAC) scoring on prospective electrocardiographically triggered 64-detctor computed tomography.

Materials and Methods. Patients ($n = 428$) suspected of having coronary artery disease were scanned twice using three protocols: with tube current modified by body mass index (BMI; group A), by BMI and body height (group B), and by attenuation at the maximal heart diameter (group C). Image noise was plotted against BMI. Interscan variability of CAC scores was determined. The effective dose was estimated by computed tomographic dose index.

Results. The mean effective dose and image noise, respectively, were 0.9 ± 0.2 mSv (range, 0.6–1.5 mSv) and 19 ± 4 Hounsfield units (HU) (range, 10–32 HU) for group A; 0.8 ± 0.2 mSv (range, 0.5–1.4 mSv) and 18 ± 4 HU (range, 10–31 HU) for group B; and 0.8 ± 0.4 mSv (range, 0.3–2.2 mSv) and 20 ± 2 HU (range, 16–26 HU) for group C. Group C used a wide dose range and controlled noise within a small range. The positive slopes of image noise versus BMI, 0.81 HU/(kg/m^2) in group A and 0.62 HU/(kg/m^2) in group B, suggested insufficient control of the tube current. In contrast, the nearly flat slope in group C, 0.091 HU/(kg/m^2), indicated optimal control. The interscan variability for Agatston score, volume, and mass in patients with CAC ($n = 300$) was 13% (median, 8%), 12% (median, 7%), and 11% (median, 6%), respectively.

Conclusions. CAC scoring on prospective electrocardiographically triggered 64-detector computed tomography using attenuation-based tube current control has the potential to favorably control image noise with low dose and low interscan variability.

Key Words. Coronary artery; calcium; tube current; attenuation; variability.

Acad Radiol 2009; 16:1231–1240

[1] From the Department of Clinical Radiology, Hiroshima University Hospital, 1-2-3, Kasumi-cho, Minami-ku, Hiroshima, 734-8551, Japan (J.H.); the Department of Radiology, Division of Medical Intelligence and Informatics (N.M., K.I.), and the Department of Cardiovascular Medicine, Hiroshima University Graduate School of Biomedical Sciences & Hiroshima University Hospital (H.Y., T.K., Y.K.), Programs for Applied Biomedicine, Graduate School of Biomedical Sciences, Hiroshima University, Minami-ku, Japan; and the Department of Environmetrics and Biometrics, Research Institute for Radiation Biology and Medicine, Hiroshima University, Minami-ku, Japan (K.S.). This study was financially supported by the Tsuchiya Foundation (Hiroshima, Japan). Received March 25, 2009; accepted April 9, 2009.
Address correspondence to: J.H. e-mail: horiguchi@hiroshima-u.ac.jp

doi:10.1016/j.acra.2009.04.008

The validity of serial coronary calcium measurements as a method to monitor the progression of atherosclerosis requires that (1) the progression of coronary artery calcium (CAC) have biologic relevance to atherosclerosis activity, (2) the progression of CAC can be detected relative to intertest variability, (3) changes in CAC severity have prognostic relevance, and (4) the modification of cardiovascular risk factors modulate the progression of CAC (1). Therefore, regarding the technical aspects of CAC scoring, low radiation exposure and low interscan variability are key requirements.

To reduce radiation exposure, a fixed and lower tube current–time product of 40 mAs (2) or 55 mAs (3) and body weight–adapted (4–6) or body mass index (BMI)–adapted (7,8) protocols have been introduced, but these do not account for the body habitus of patients, such as the

size of heart or the presence of pericardial effusion. In a recent report of the International Consortium on Standardization in Cardiac Computed Tomography, a standard deviation (SD) level target of 20 Hounsfield units (HU) for small and medium-sized patients and an SD level target of 23 HU for large patients have been recommended (9). Mühlenbruch et al (10) reported automated attenuation-based tube current adaptation whereby the tube current was chosen from a proprietary control curve calculated on the basis of the attenuation values derived from the scanogram. Their study showed that automated attenuation-based tube current adaptation can better control tube current than a fixed "standard" dose protocol, but their regression analysis revealed a statistically significant influence of patient BMI on image noise.

We hypothesized that tube current should be adjusted by attenuation at the level of the maximal heart diameter on the scout image. Moreover, prospective electrocardiographically triggered scans should be used for the reduction of radiation dose. Thus, the main purpose of this prospective study was to investigate image noise and to assess variability in repeated CAC scoring on prospective electrocardiographically triggered 64-detector computed tomographic (CT) imaging using attenuation-based tube current adaptation at the maximal heart diameter. We also compared this protocol to two other protocols: tube current modified by BMI (8) and tube current modified by BMI and body height.

MATERIALS AND METHODS

Patients

For 24 months, 428 consecutive subjects (261 men, 167 women; mean age, 65 ± 12 years; age range, 28–89 years) who underwent coronary CT imaging for coronary risk factors or chest pain evaluation were enrolled in the study and were classified into three groups. Patients with histories of cardiac surgery, stents, or pacemakers were excluded. Study participants were collected until each group reached 100 patients with CAC. Consequently, groups A, B, and C consisted of 145, 145, and 138 patients, respectively. The study was approved by our institutional review committee. Written informed consent was received from all patients involved after the nature of the procedure had been fully explained (including radiation dose information).

Prospective Electrocardiographically Triggered Step-and-Shoot CT Protocol

Two repeated prospective electrocardiographically triggered step-and-shoot half scans were performed using a 64-detector CT scanner (LightSpeed VCT; GE Healthcare, Waukesha, WI) with simultaneous electrocardiographic digitizing and recording. Between the two scans, to simulate different body positions, the table was advanced by 1 mm. Scans were performed 4 to 5 seconds after holding the breath on mild inspiration to minimize changes in heart rate during the scans (11). Using a collimation width of 2.5 mm and 16 detectors, images of 2.5 mm in thickness were obtained. Scans were temporally triggered to be centered at 75% of the RR interval, because middiastolic reconstruction has been recommended on 64-detector CT scanners with gantry rotation speed of 0.35 seconds (12). The gantry rotation speed was 0.35 seconds, and the tube voltage was 120 kV. For image reconstruction parameters, a matrix size of 512 × 512 pixels, a display field of view of 26 cm, and the "standard" kernel were used. The temporal resolution was 175 ms.

Group A: Tube Current Modified by BMI

Group A consisted of subjects reported in a previous paper (8) plus 30 subjects. Because a significant association between noise and BMI was shown in an electron-beam CT study (7), the tube current was modified according to the following equation:

$$\text{tube current} = 250 \times (\text{BMI}/25)$$

$$\text{mA} = 10 \times \text{body weight (kg)} / [\text{body height (m)}]^2 \text{ mA}.$$

This was based on the strategy that patients with standard BMIs of 25 kg/m^2 would receive tube current–time product of 58 mAs, which is almost the same level as the recommendation for CAC scoring using low-dose 4-slice CT imaging (3).

The tube current–time product in a typical patient with a BMI of 25 kg/m^2 was calculated as follows:

$$\text{tube current (mA)} \times \text{gantry rotation speed (seconds)} \times \text{exposure time per rotation time} = 250 \text{ mA} \times 0.35 \text{ seconds} \times (2/3) = 58 \text{ mAs}.$$

Group B: Tube Current Modified by BMI and Body Height

In addition to BMI, this protocol considered the influence of body height. The tube current was modified according to the following equation:

$$\text{tube current} = 250 \times (\text{BMI}/25) \text{ mA} \times (\text{body height}/1.7) \text{ mA} = 5.88 \times \text{body weight (kg)} / \text{body height (m)} \text{ mA}.$$

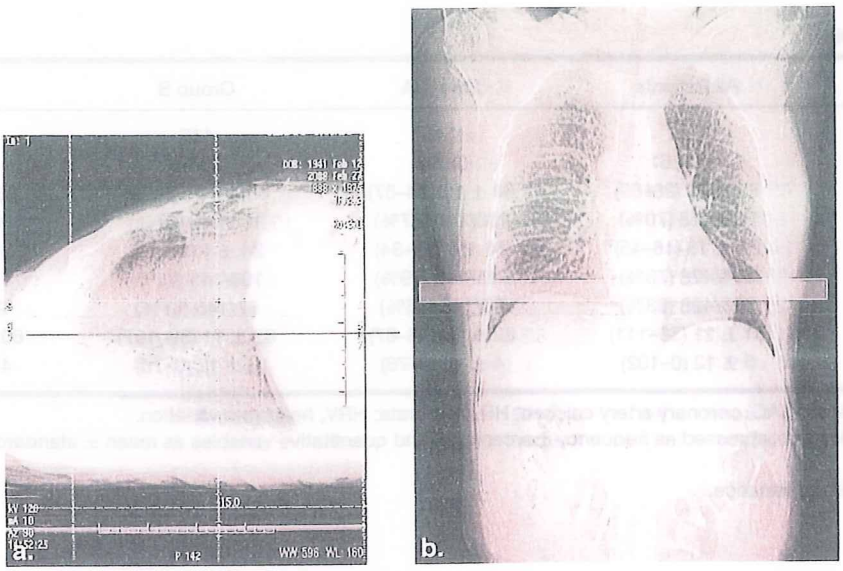

Figure 1. Attenuation-based tube current adaptation at the maximal heart diameter. First, the lateral scout view is taken **(a)**. The grids *(dotted lines)* show that the isocenter of the x-ray beam is 2 cm higher than the center of body *(black line)* in the ventral-dorsal direction at the left ventricular level. The table is elevated by 2 cm so that the isocenter of the x-ray beam and the center of the body correspond. Next, the frontal scout view is taken. The z-axis level of the maximal heart diameter on the frontal scout view is chosen **(b)**, and a targeted noise level of 20 HU is input into the software Smart mA. Then, a recommended value for the tube current is displayed. Because this value is offered on the simulation of a full scan and a gantry rotation speed of 0.4 seconds, the tube current for coronary artery calcium scanning is determine according to the following equation: tube current = recommended tube current × (3/2) × (0.4/0.35) mA.

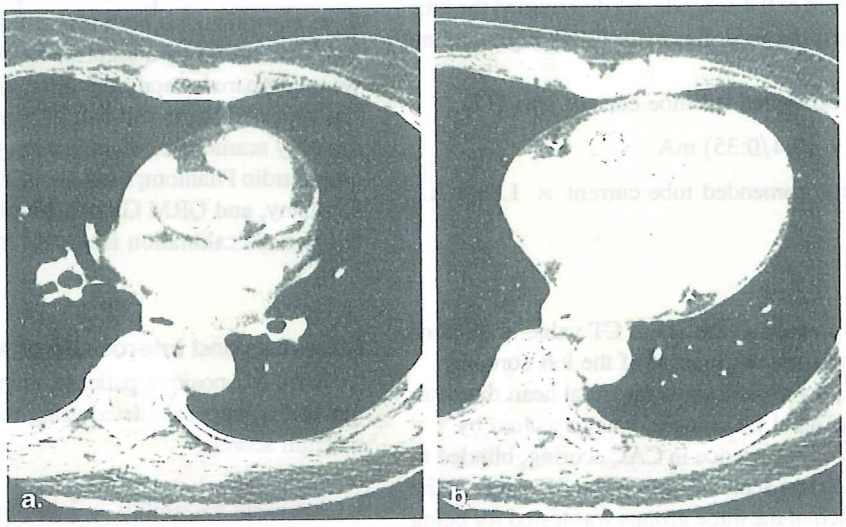

Figure 2. Image noise measurement. Image noise expressed as the standard deviation of computed tomographic (CT) values is measured in regions of interest set in the aorta at the level of the left coronary artery **(a)** and in the right ventricle at the maximal heart diameter level determined on axial CT images **(b)**.

Table 1
Patient Demographics

Variable	All Patients	Group A	Group B	Group C	*P*
No. of patients	428	145	145	138	.48†
Women/women	167/261	52/93	60/85	55/83	.43‡
Age (y)	65 ± 12 (28–89)	64 ± 12 (34–87)	65 ± 13 (28–89)	66 ± 11 (31–85)	.52†
Prevalence of CAC	300/428 (70%)	100/145 (67%)	100/145 (67%)	100/138 (72%)	.27‡
BMI (kg/m^2)	24 ± 13 (16–45)	24 ± 3 (18–34)	24 ± 4 (16–40)	24 ± 3 (16–32)	.95†
Symptoms	334/428 (78%)	115/145 (79%)	109/145 (75%)	110/138 (80%)	.06‡
Risk factors	268/428 (63%)	80/145 (55%)	97/145 (67%)	91/138 (66%)	.47‡
HR (beats/min)*	61 ± 11 (38–111)	62 ± 10 (40–87)	62 ± 11 (39–107)	60 ± 12 (38–111)	.44†
HRV (beats/min)*	5 ± 12 (0–102)	4 ± 10 (0–76)	6 ± 12 (0–75)	4 ± 14 (0–102)	.48†

BMI, body mass index; CAC, coronary artery calcium; HR, heart rate; HRV, heart rate variation.
Categorical variables are expressed as frequency (percentage) and quantitative variables as mean ± standard deviation (range).
* Data in scan 1.
† One-factor analysis of variance.
‡ Chi-square test.

Group C: Attenuation-Based Tube Current Adaptation at the Maximal Heart Diameter

Because this protocol used attenuation-based tube current adaptation, we set the isocenter of the x-ray beam to adjust the center of body in the ventral-dorsal direction at the left ventricular level. First, we took a lateral scout image and, if necessary, reset the position of the table so that the isocenter of x-ray beam and the center of body corresponded (Fig 1a). Next, we took a frontal scout image. We determined the z-axis level of the maximal heart diameter on the frontal scout view (Fig 1b) and input a targeted noise level of 20 HU in the software Smart (Advantage windows version 4.2) mA; thereafter, a value of tube current was recommended. Because this value was offered on the simulation of a full scan and a gantry rotation speed of 0.4 seconds, we determined the tube current for CAC scanning according to the following equation:

$$\begin{aligned}\text{tube current} &= \text{recommended tube current} \times (3/2) \\ &\quad \times (0.4/0.35)\ \text{mA} \\ &= \text{recommended tube current} \times 1.71\ \text{mA}.\end{aligned}$$

Image Noise

Image noise, expressed as the SD of CT value, in regions of interest set in the aorta at the level of the left coronary artery and in the right ventricle at the maximal heart diameter level determined on axial CT images, was measured by observer 1 (9 years of experience in CAC scoring, blinded to patients' information) on scan 1 (Fig 2). The SD value in the right ventricle of each of the three groups was tested for being equal to 20 HU. The mean + 2 SDs of CT values in the two regions of interest, preferably lower than the threshold of 130 HU (7), was calculated. To investigate the relationship between SD and BMI, the SD was plotted against BMI, as described by Mahnken et al (4).

Calcium Scoring

The Agatston score (13) and calcium volume and mass (14) were determined using a commercially available external workstation (Advantage Windows version 4.2; GE Healthcare) and CAC-scoring software (Smartscore version 3.5; GE Healthcare).

All CT scans were independently scored by two radiologists blinded to patients' information, with 9 and 3 years of experience in CAC scoring (observers 1 and 2, respectively). We defined "CAC positive" as positive CAC scores for the three algorithms on both scans. For CAC-positive patients, the CAC scores on a logarithmic scale (to reduce skewness) were compared among the three groups, as well as between two repeated scans and two observers. We performed monthly scanning of a calibration phantom (Anthropomorphic Cardio Phantom; Institute of Medical Physics, Erlangen, Germany, and QRM GmbH, Möhrendorf, Germany) to determine the calibration factor for mass score (15).

Interscan and Interobserver Variability

For CAC-positive patients, interscan and interobserver variability were calculated using the percentage difference in calcium scores:

$$\begin{aligned}\text{interscan variability} &= [\text{absolute}(\text{scan 1} - \text{scan 2})/ \\ &\quad (\text{scan 1} + \text{scan 2}) \times 0.5] \\ &\quad \times 100,\end{aligned}$$

and

Table 2
Image Noise in the Ascending Aorta and Right Ventricle

Variable	All Patients	Group A	Group B	Group C
No. of patients	428	145	145	138
SD (HU)				
Ascending aorta	17 ± 7 (11–30)	16 ± 3 (11–27)	17 ± 3 (11–30)	17 ± 2 (12–24)
Right ventricle	19 ± 4 (10–32)	19 ± 4 (10–32)	18 ± 4 (10–31)	20 ± 2 (16–26)
Mean + 2 SDs (HU)				
Ascending aorta	75 ± 9 (53–109)	75 ± 10 (53–99)	75 ± 10 (53–109)	76 ± 7 (57–100)

HU, Hounsfield units; SD, standard deviation.
Data are expressed as mean ± SD (range).

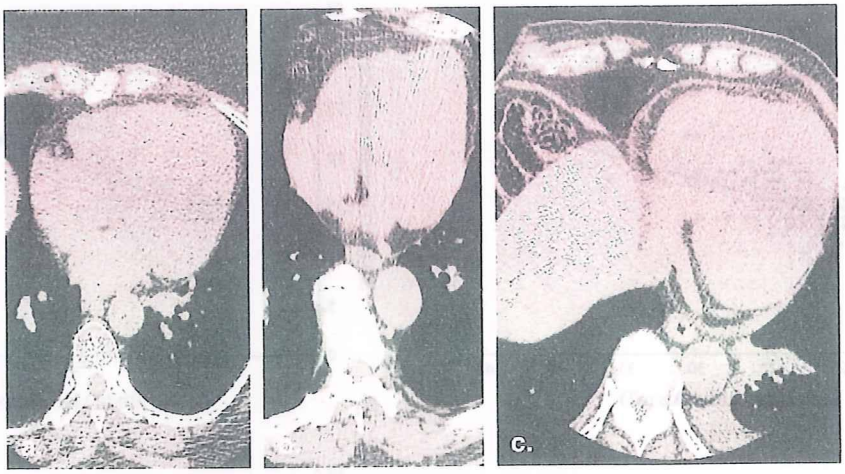

Figure 3. The highest standard deviation images in the three groups. Images with the highest noise in the three groups are shown. **(a)** An image of a 57-year-old woman (body mass index [BMI], 34.1 kg/m^2; body height, 155 cm) below the diaphragm level (SD = 32 Hounsfield units [HU]). **(b)** An image of a 57-year-old man (BMI, 27.1 kg/m^2; body height, 165 cm) was sacrificed to streaking artifact from spinal spur (SD = 31 HU). **(c)** An image of an 80-year-old man (BMI, 26.8 kg/m^2; body height, 164 cm) below the diaphragm shows pleural and pericardial effusion (SD = 26 HU).

$$\text{interobserver variability} = [\text{absolute}(\text{observer 1} - \text{observer 2})/(\text{observer 1} + \text{observer 2}) \times 0.5] \times 100,$$

where observer 1 and observer 2 are the CAC scores measured by the respective observers. Interscan variability, on a logarithmic scale, was compared among the three groups and CAC-scoring algorithms.

Radiation Dose

The dose-length product (in milligrays by centimeter) displayed on the dose report on the CT scanner was recorded. The effective dose was estimated by a method proposed by the European Working Group for Guidelines on Quality Criteria in Computed Tomography [16]. In this method, the effective dose is derived from the dose-length product and a conversion coefficient for the chest (k = 0.017 mSv/mGy/cm averaged between male and female models). The effective doses in the three groups were plotted against BMI.

Statistical Analyses

All statistical analyses were performed using commercially available software package (MedCalc 9.5.1 for Windows; MedCalc Software, Mariakerke, Belgium). Categorical variables are presented as frequencies and percentages and continuous variables as mean ± SD. The χ^2 and analysis of variance (ANOVA; multivariate calculations)

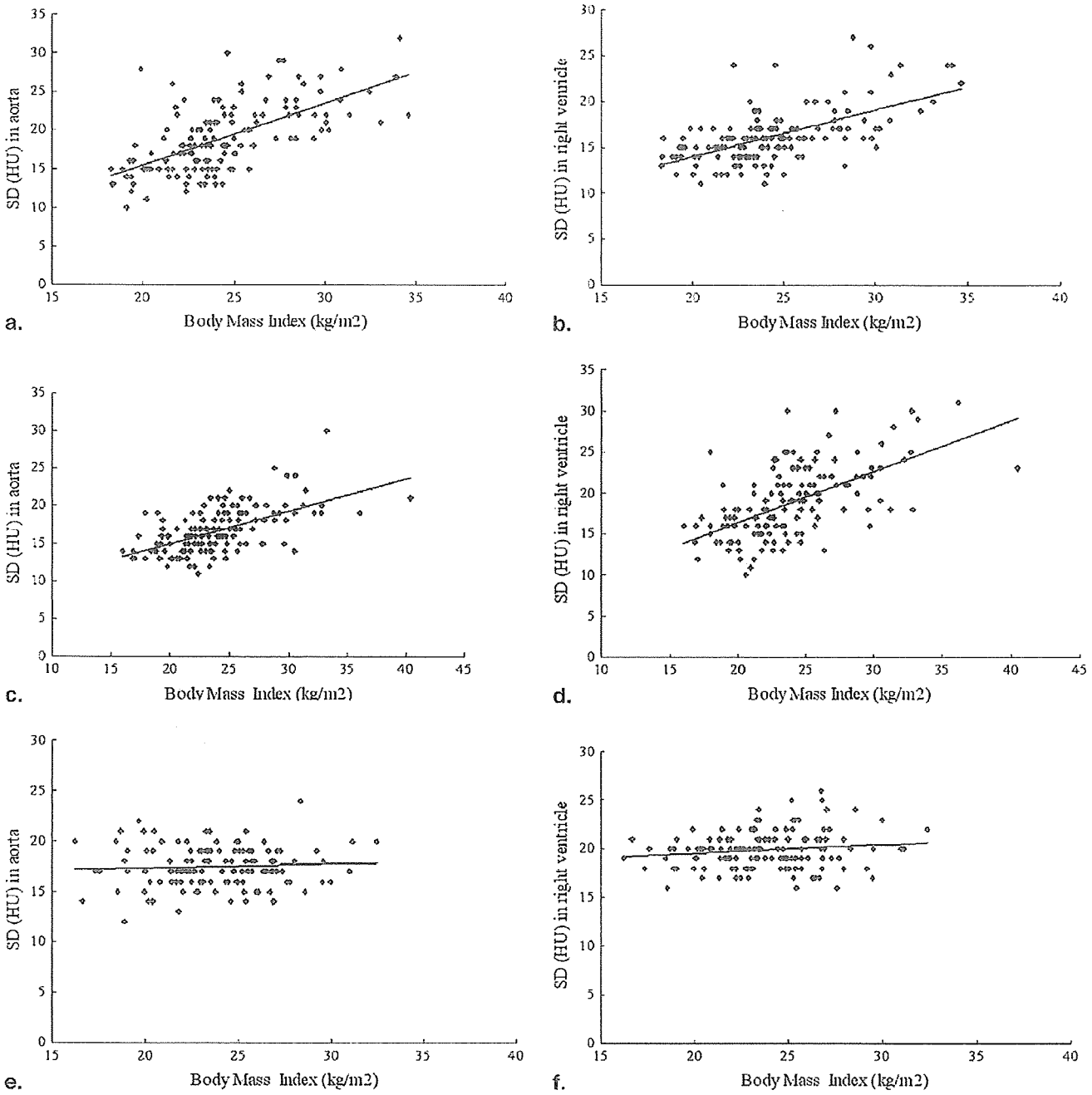

Figure 4. The relationship between standard deviation (SD) and body mass index (BMI). Scatterplots show the ratio between BMI (kg/m^2) and SD (Hounsfield units [HU]). **(a)** Group A, in the aorta: SD = 0.51 (95% confidence interval [CI], 0.40–0.62) × BMI + 4 ($P < .01$). **(b)** Group A, in the right ventricle: SD = 0.81 (95% CI, 0.64–0.97) × BMI − 1 ($P < .01$). **(c)** Group B, in the aorta: SD = 0.43 (95% CI, 0.33–0.53) × BMI + 6 ($P < .01$). **(d)** Group B, in the right ventricle: SD = 0.62 (95% CI, 0.48–0.76) × BMI + 4 ($P < .01$). **(e)** Group C, in the aorta: SD = 0.041 (95% CI, −0.069 to 0.15) × BMI + 16 (P = .46). **(f)** Group C, in the right ventricle: SD = 0.091 (95% CI, −0.013 to 0.20) × BMI + 18 ($P = .09$). The positive slopes of image noise versus BMI, 0.51 and 0.81 HU/(kg/m^2) in group A and 0.43 and 0.62 HU/(kg/m^2) in group B, suggest insufficient control of the tube current. In contrast, the nearly flat slopes of 0.041 and 0.091 HU/(kg/m^2) in group C indicate optimal control of tube current across patients.

Table 3
Coronary Artery Calcium Scores and Interscan and Interobserver Variability

Variable	All Patients	Group A	Group B	Group C
No. of patients	300	100	100	100
Agatston score				
Scan 1				
Observer 1	175 (48, 648)	206 (46, 664)	167 (42, 464)	152 (48, 775)
Observer 2	185 (48, 648)	206 (48, 668)	174 (42, 488)	157 (48, 789)
Scan 2				
Observer 1	179 (43, 610)	201 (46, 638)	171 (42, 444)	148 (39, 797)
Observer 2	176 (45, 611)	204 (46, 638)	176 (42, 462)	148 (39, 803)
Volume score				
Scan 1				
Observer 1	150 (43, 515)	165 (38, 548)	138 (39, 367)	125 (44, 639)
Observer 2	149 (43, 528)	166 (40, 552)	146 (37, 392)	129 (44, 622)
Scan 2				
Observer 1	144 (41, 502)	176 (39, 502)	144 (35, 356)	122 (41, 665)
Observer 2	146 (41, 502)	176 (40, 502)	146 (36, 366)	121 (41, 668)
Calcium mass				
Scan 1				
Observer 1	33 (8, 127)	37 (8, 130)	30 (7, 93)	28 (8, 139)
Observer 2	33 (8, 130)	37 (8, 132)	30 (7, 93)	28 (8, 139)
Scan 2				
Observer 1	32 (8, 123)	37 (8, 131)	30 (7, 89)	25 (7, 153)
Observer 2	32 (8, 123)	37 (8, 131)	30 (6, 91)	26 (7, 149)
Interscan variability (%)				
Agatston				
Observer 1	13, 8 (3, 17)	13, 7 (2, 15)	12, 6 (2, 15)	14, 10 (4, 18)
Observer 2	13, 8 (3, 17)	13, 7 (3, 16)	13, 6 (2, 16)	14, 10 (3, 20)
Volume				
Observer 1	12, 7 (3, 16)	12, 6 (3, 16)	11, 6 (2, 15)	11, 8 (3, 15)
Observer 2	11, 6 (3, 16)	11, 6 (2, 15)	10, 6 (2, 15)	12, 8 (3, 17)
Mass				
Observer 1	11, 6 (2, 14)	10, 4 (2, 14)	10, 5 (2, 11)	12, 8 (2, 14)
Observer 2	11, 6 (2, 14)	10, 4 (2, 14)	12, 5 (2, 11)	11, 8 (2, 14)
Interobserver variability (%)				
Agatston				
Scan 1	4, 1 (0, 3)	3, 1 (0, 4)	5, 0 (0, 3)	3, 0 (0, 2)
Scan 2	3, 0 (0, 3)	5, 0 (0, 3)	4, 0 (0, 2)	2, 1 (0, 1)
Volume				
Scan 1	2, 0 (0, 2)	3, 0 (0, 3)	3, 0 (0, 1)	1, 0 (0, 0)
Scan 2	2, 0 (0, 2)	3, 0 (0, 2)	4, 0 (0, 2)	1, 0 (0, 3)
Mass				
Scan 1	3, 1 (0, 1)	3, 0 (0, 2)	4, 0 (0, 2)	1, 0 (0, 1)
Scan 2	3, 0 (0, 1)	3, 0 (0, 2)	4, 0 (0, 1)	2, 0 (0, 1)

Coronary artery calcium is expressed as median (25th, 75th percentiles). Variability is expressed as mean, median (25th, 75th percentiles).

tests were used to determine group differences. P values $< .05$ were considered to identify significant differences.

RESULTS

All patients were able to hold their breath for the two scans. Baseline characteristics of the patients are presented in Table 1. Neither heart rate ($P = .47$) nor heart rate variation ($P = .44$) was different among the three groups. Three hundred of the overall 428 patients were CAC positive. One hundred twenty patients showing negative scores on both scans and eight patients showing both positive and negative scores between scans or between algorithms were excluded for the calculation of variability.

Table 4
Tube Current, Tube Current–Time Product, and Radiation Dose

Variable	All Patients	Group A	Group B	Group C	P
Tube current (mA)	227 ± 65 (75–610)	245 ± 36 (180–350)	227 ± 43 (150–370)	209 ± 94 (75–610)	<.01*
Tube current–time product (mAs)	53 ± 15 (18–142)	57 ± 8 (42–56)	53 ± 10 (35–86)	49 ± 25 (18–142)	<.01*
Dose0length product (mGy · cm)	49 ± 15 (16–131)	53 ± 8 (37–87)	49 ± 10 (30–84)	44 ± 21 (16–131)	<.01*
Estimate effective dose (mSv)	0.8 ± 0.3 (0.3–2.2)	0.9 ± 0.2 (0.6–1.5)	0.8 ± 0.2 (0.5–1.4)	0.8 ± 0.4 (0.3–2.2)	<.01*

Data are expressed as mean ± standard deviation (range).
* One-factor analysis of variance.

Image Noise

The SD and the mean + 2 SDs in regions of interest in the aorta and the right ventricle are presented in Table 2. The test for one mean revealed that the SD in the right ventricle was different from 20 HU in group A (95% confidence interval [CI], 18.3–19.7; $P < .01$) and group B (95% CI, 17.3–18.7; $P < .01$), whereas the SD was not different from 20 HU in group C (95% CI, 19.7–20.3; $P = 1.00$). In group C, the mean SD was 20 ± 2 HU (range, 16–26 HU). Images with the highest noise in the three groups are shown in Figure 3. In group C, six of 138 patients (4%) showed CT values > 23 HU in the right ventricle (at the maximal heart diameter level on the axial CT image). In five of the patients, the image levels were below the dome of the diaphragm, being different from the image used for the measurement of attenuation in the scout image.

The mean + 2 SDs did not exceed 130 HU in groups A and C, whereas the value in the right ventricle was 133 HU in one case in group B.

The regression analysis revealed a statistically significant influence of patient BMI on image noise in groups A and B (Figs 4a–d). In group C, however, nearly flat slopes of 0.04 and 0.091 HU/(kg/m^2) were seen between BMI and SD, indicating favorable control of tube current (Figs 4e and 4f).

CAC Scores and Interscan and Interobserver Variability

CAC scores and the interscan and interobserver variability are summarized in Table 3. The CAC scores were not different among the three groups. For a representative example, one-factor ANOVA revealed that there was no significant difference of log-transformed Agatston scores on scan 1 measured by observer 1 between the groups ($P = .61$). CAC scores were not different between scans and observers; for example, repeated-measures ANOVA revealed that there was no statistical significance of log-transformed Agatston scores in group A between the scans ($P = .31$) and observers ($P = .91$).

For observer 1, the mean interscan variability of CAC-positive patients in all groups ($n = 300$) was 13% (median, 8%) for Agatston score, 12% (median, 7%) for volume, and 11% (median, 6%) for mass. Two-factor ANOVA revealed that the interscan variability in CAC scores, on a logarithmic scale, was not different among the three groups ($P = .17$) and algorithms ($P = .07$).

Interobserver variability was small. For scan 1, the mean interobserver variability for Agatston score, volume, and mass in CAC-positive patients was 4% (median, 1%), 2% (median, 0%) and 3% (median, 1%), respectively.

Radiation Dose

The tube currents, tube current–time products, dose-length products, and estimated effective doses in the 3 groups are shown in Table 4. One-factor ANOVA revealed that there were significant differences in all values among the three groups ($P < .01$). Group C used the least dose and, more important, a wide range of doses (effective dose, 0.3–2.2 mSv). The plots of effective dose against BMI are shown in Figures 5a to 5c. In group C, the tube currents used and radiation doses were different among individuals and widely distributed compared with groups A and B.

DISCUSSION

The major points of the present study are as follows: (1) attenuation-based tube current control, at the level of the maximal heart diameter on the scout view, has the potential to favorably control image noise in CAC scoring; (2) low-dose scanning is possible, combined with prospective electrocardiographically triggered scanning; and (3) the protocol for 64-detector CT imaging provides low interscan and interobserver variability.

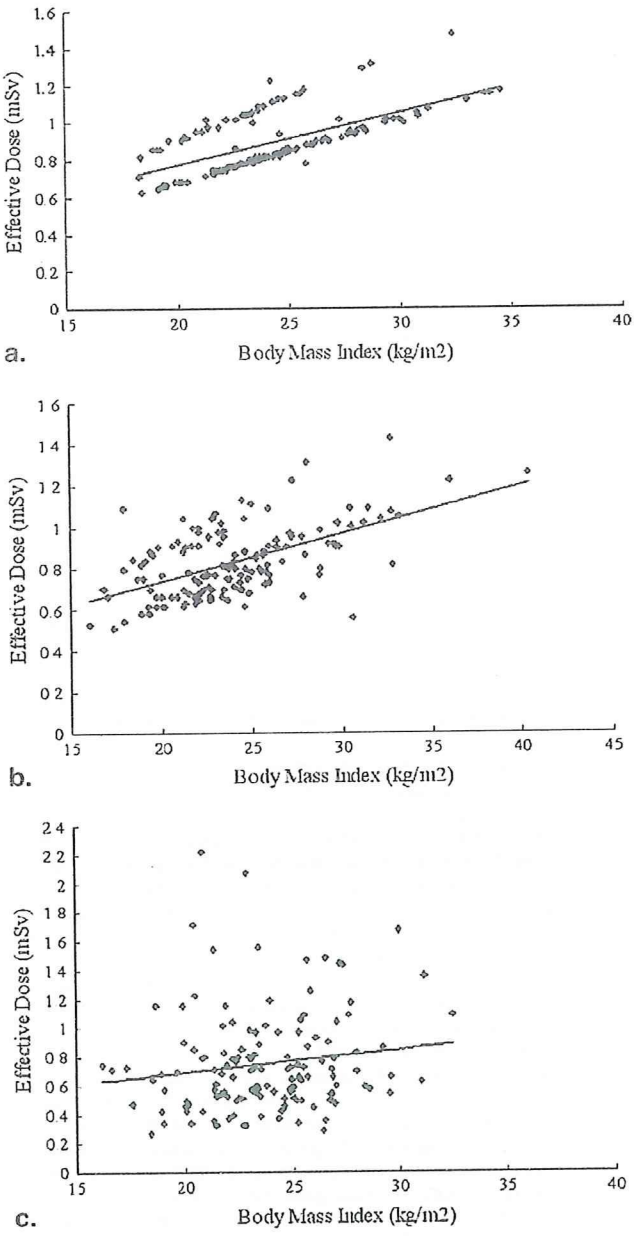

Figure 5. The relationship between effective dose and body mass index (BMI). Plots of effective dose against BMI are shown. **(a)** Group A: effective dose = 0.028 × BMI + 0.22 ($P < .01$). **(b)** Group B: effective dose = 0.023 × BMI + 0.27 ($P < .01$). **(c)** Group C: effective dose = 0.016 × BMI + 0.38 ($P = .11$). In groups A and B, effective dose was a function of BMI, but not in group C. The effective doses in group C were widely distributed, irrespective of BMI values.

Image Noise

In attenuation-based tube current control, the mean noise was controlled to the target value of 20 HU. In addition, the range was small compared to the BMI group and BMI and body height group. These facts indicate that attenuation-based scanning meets the goal of dose that is as low as reasonably achievable. Of the 138 patients in the attenuation-based group, the maximal mean + 2 SDs was 107 HU in the right ventricle. Because the CT value threshold of CAC detection was set to 130 HU, this result indicates that the noise is not likely to be falsely judged as CAC. This is also important because image noise is known to be one factor affecting interscan variability of CAC (17,18). In the BMI and BMI and body height groups, image noise was a function of BMI, suggesting insufficient control of the tube current in individual patients. Although an increase in body weight or BMI theoretically leads to an increase in image noise, the noise cannot be ideally controlled on the basis of these parameters.

Interscan and Interobserver Variability in CAC Scoring

The interscan variability of Agatston scores in 300 CAC-positive patients (for observer 1: mean, 13%; median, 8%) was lower than the variability on electron-beam CT imaging (20%–37%) (14,17,19,20) and was comparable to the variability on overlapping images from retrospective reconstruction on prior-generation (4-slice or 16-slice) multidetector CT imaging (21,22). The variability was also comparable to that on 64-detector CT imaging (23). However, the data on 64-detector CT imaging are from a single institution. It is our hope that more data from multiple institutions will be collected. Apart from overlapping images, the use of a volume or mass algorithm can further reduce variability. Although not significant ($P = .07$), this trend was observed in the present study, in line with previous studies (22,23). The interobserver variability in this study was small. Artificial lesions, known to affect interobserver variability, were reduced in the study, with favorably controlled noise. We consider the interscan and interobserver variability in the current study encouraging. However, prudence is called for in actual clinical practice, because patients are likely to have different heart rates when studies are performed a few years apart, and body habitus and position may also change, thus possibly increasing variability.

Radiation Dose

In the attenuation-based group, the tube currents and associated radiation doses were distributed over a wide range, and the doses were different even among patients with the same BMIs. This is considered an appropriate method in patients who do not require much dose (eg, slender patients who do not receive more dose than necessary). For example, the minimal dose was only 0.3 mSv for a small and slender patient (height, 151 cm; weight, 42 kg; BMI, 18 kg/m^2). We also found that the mean radiation dose in the attenuation-based group was the same as on electron-beam CT imaging (0.7 mSv) (24). We may therefore conclude that this level of

radiation dose may be suited for repeated examination to monitor the progression of atherosclerosis. Another approach for the reduction of dose is lowering the tube voltage (25,26). However, this requires need calibration for the calculation of a scanner with a specifically adapted threshold for the identification of calcium and is available only for calcium mass scoring.

A technical issue should be addressed. Because the current was determined at the maximal heart diameter on the scout view, image noise below the dome of the diaphragm tended to become higher. Indeed, five patients showed CT values > 23 HU in the right ventricle below the dome of the diaphragm. However, considering that the largest part of the coronary arteries was suggested to exist in the first 6 cm of the transverse scan (27), CAC below the diaphragmatic level is probably of less importance. Although we could have controlled the image noise by adjusting at such a lower level, we did not choose to do so, because it might have excessively increased radiation dose.

One limitation is that this study was conducted at a single institution in Japan, and the participants consisted of smaller patients than typical US citizens, resulting in a lower estimated dose than expected for US citizens. Nevertheless, the method is applicable to any patient and seems promising for the control of tube current in CAC scoring.

In conclusion, attenuation-based tube current control at the level of the maximal heart diameter on the scout view has the potential to favorably control image noise across patients. Low dose and low interscan variability on CAC scoring are shown on prospective electrocardiographically triggered 64-detector CT imaging.

REFERENCES

1. Greenland P, Bonow RO, Brundage BH, et al. ACCF/AHA 2007 clinical expert consensus document on coronary artery calcium scoring by computed tomography in global cardiovascular risk assessment and in evaluation of patients with chest pain. J Am Coll Cardiol 2007; 49: 378–402.
2. Takahashi N, Bae KT. Quantification of coronary artery calcium with multi-detector row CT: assessing interscan variability with different tube currents-pilot study. Radiology 2003; 228:101–106.
3. Shemesh J, Evron R, Koren-Morag N, et al. Coronary artery calcium measurement with multi-detector row CT and low radiation dose: comparison between 55 and 165 mAs. Radiology 2005; 236:810–814.
4. Mahnken AH, Wildberger JE, Simon J, et al. Detection of coronary calcifications: feasibility of dose reduction with a body weight-adapted examination protocol. AJR Am J Roentgenol 2003; 181:533–538.
5. Jung B, Mahnken AH, Stargardt A, et al. Individually weight-adapted examination protocol in retrospectively ECG-gated MSCT of the heart. Eur Radiol 2003; 13:2560–2566.
6. Horiguchi J, Yamamoto H, Hirai N, et al. Variability of repeated coronary artery calcium measurements on low-dose ECG-gated 16-MDCT. AJR Am J Roentgenol 2006; 187:W1–W6.
7. Sevrukov A, Pratap A, Doss C, Jelnin V, Hoff JA, Kondos GT. Electron beam tomography imaging of coronary calcium: the effect of body mass index on radiologic noise. J Comput Assist Tomogr 2002; 26:592–597.
8. Horiguchi J, Matsuura N, Yamamoto H, et al. Coronary artery calcium scoring on low-dose prospective electrocardiograph-triggered 64-slice CT. Acad Radiol 2009; 16:187–193.
9. McCollough CH, Ulzheimer S, Halliburton SS, et al. Coronary artery calcium: a multiinstitutional, multimanufacturer international standard for quantification at cardiac CT. Radiology 2007; 243:527–538.
10. Mühlenbruch G, Hohl C, Das M, et al. Evaluation of automated attenuation-based tube current adaptation for coronary calcium scoring in MDCT in a cohort of 262 patients. Eur Radiol 2007; 17:1850–1857.
11. Horiguchi J, Shen Y, Hirai N, et al. Timing on 16-slice scanner and implications for 64-slice cardiac CT: do you start scanning immediately after breath-hold? Acad Radiol 2006; 13:173–176.
12. Matsuura N, Horiguchi J, Yamamoto H, et al. Optimal cardiac phase for coronary artery calcium scoring on single-source 0.35 sec-rotation-speed 64-MDCT scanner—least interscan variability and least motion artifacts. AJR Am J Roentgenol 2008; 190:1561–1568.
13. Agatston AS, Janowitz WR, Hildner FJ, Zusmer NR, Viamonte M, Detrano R. Quantification of coronary calcium using ultrafast computed tomography. J Am Coll Cardiol 1990; 15:827–832.
14. Yoon HC, Greaser LE III, Mather R, Sinha S, McNitt-Gray MF, Goldin JG. Coronary artery calcium: alternate methods for accurate and reproducible quantitation. Acad Radiol 1997; 4:666–673.
15. Halliburton SS, Stillman AE, Lieber M, Kasper JM, Kuzmiak SA, White RD. Potential clinical impact of variability in the measurement of coronary artery calcification with sequential MDCT. AJR Am J Roentgenol 2005; 184:643–648.
16. Menzel H, Schibilla H, Teunen D. European guidelines for quality criteria for computed tomography. Brussels, Belgium: European Commission, 2000.
17. Achenbach S, Ropers D, Mohlenkamp S, et al. Variability of repeated coronary artery calcium measurements by electron beam tomography. Am J Cardiol 2001; 87:210–213.
18. Bielak LF, Kaufmann RB, Moll PP, MacCollough CH, Schwartz RS, Sheedy PF II. Small lesions in the heart identified at electron beam CT: calcification or noise? Radiology 1994; 192:631–636.
19. Callister TQ, Cooil B, Raya SP, et al. Coronary artery disease: improved reproducibility of calcium scoring with an electron-beam CT volumetric method. Radiology 1998; 208:807–814.
20. Wang SJ, Detrano BC, Secci A, et al. Detection of coronary calcification with electron-beam computed tomography: evaluation of interexamination reproducibility and comparison of three image-acquisition protocols. Am Heart J 1996; 132:550–558.
21. Ohnesorge B, Flohr T, Fischbach R, et al. Reproducibility of coronary calcium quantification in repeat examinations with retrospectively ECG-gated multisection spiral CT. Eur Radiol 2002; 12:1532–1540.
22. Horiguchi J, Yamamoto H, Akiyama Y, et al. Variability of repeated coronary artery calcium measurements by 16-MDCT with retrospective reconstruction. AJR Am J Roentgenol 2005; 184:1917–1923.
23. Horiguchi J, Matsuura N, Yamamoto H, et al. Variability of repeated coronary artery calcium measurements by 1.25-mm- and 2.5-mm-thickness images on prospective electrocardiograph-triggered 64-slice CT. Eur Radiol 2008; 18:209–216.
24. Morin RL, Gerber TC, McCollough CH. Radiation dose in computed tomography of the heart. Circulation 2003; 107:917–922.
25. Thomas CK, Mühlenbruch G, Wildberger JE, et al. Coronary artery calcium scoring with multislice computed tomography. in vitro assessment of a low tube voltage protocol. Invest Radiol 2006; 41:668–673.
26. Jakobs TF, Wintersperger BJ, Herzog P, et al. Ultra-low-dose coronary artery calcium screening using multislice CT with retrospective ECG gating. Eur Radiol 2003; 13:1923–1930.
27. Vliegenthart R, Song B, Hofman A, Witteman JCM, Oudkerk M. Coronary calcification at electron-beam CT: effect of section thickness on calcium scoring in vitro and in vivo Radiology 2003; 229:520–525.

G Model
EURR-4516; No. of Pages 5

European Journal of Radiology xxx (2009) xxx–xxx

Contents lists available at ScienceDirect

European Journal of Radiology

journal homepage: www.elsevier.com/locate/ejrad

In vitro measurement of CT density and estimation of stenosis related to coronary soft plaque at 100 kV and 120 kV on ECG-triggered scan

Jun Horiguchi[a,*], Chikako Fujioka[a], Masao Kiguchi[a], Hideya Yamamoto[b], Yun Shen[c], Yasuki Kihara[b]

[a] Department of Clinical Radiology, Hiroshima University Hospital, 1-2-3, Kasumi-cho, Minami-ku, Hiroshima 734-8551, Japan
[b] Department of Cardiovascular Medicine, Hiroshima University Graduate School of Biomedical Sciences & Hiroshima University Hospital, 1-2-3, Kasumi-cho, Minami-ku, Hiroshima 734-8551, Japan
[c] CT Lab of Great China, GE Healthcare, L12&L15, Office Tower, Langham Place, 8 Argyle Street, Mongkok Kowloon, Hong Kong

ARTICLE INFO

Article history:
Received 3 June 2009
Accepted 3 August 2009

Keywords:
100 kV
Prospective ECG-triggered
Axial
Coronary
Soft plaque

ABSTRACT

Purpose: The purpose of the study was to compare 100 kV and 120 kV prospective electrocardiograph (ECG)-triggered axial coronary 64-detector CT angiography (64-MDCTA) in soft plaque diagnosis.
Materials and methods: Coronary artery models ($n = 5$) with artificial soft plaques (−32 HU to 53 HU at 120 kV) with three stenosis levels (25%, 50% and 75%) on a cardiac phantom (mimicking slim patient's environment) were scanned in heart rates of 55, 60 and 65 beats per minute (bpm). Four kinds of intracoronary enhancement (205 HU, 241 HU, 280 HU and 314 HU) were simulated. The soft plaque density and the measurement error of stenosis (in percentage), evaluated by two independent observers, were compared between 100 kV and 120 kV. The radiation dose was estimated.
Results: Interobserver correlation of the measurement was excellent (density; $r = 0.95$ and stenosis measure; $r = 0.97$). Neither the density of soft plaque nor the measurement error of stenosis was different between 100 kV and 120 kV ($p = 0.22$ and 0.08). The estimated radiation doses were 2.0 mSv and 3.3 mSv (in 14 cm coverage) on 100 kV and 120 kV prospective ECG-triggered axial scans, respectively.
Conclusion: The 100 kV prospective ECG-triggered coronary MDCTA has comparable performance to 120 kV coronary CTA in terms of soft plaque densitometry and measurement of stenosis, with a reduced effective dose of 2 mSv.

1. Introduction

Ruptured plaque, a trigger of acute coronary syndrome, is histopathologically characterized by large plaque volume and a large necrotic core that are covered by an attenuated fibrous cap often inflamed with macrophage infiltration [1]. The rupture-prone plaque, which is seven times more likely to ulcerate than the more severe, extensive plaque, is not visible on 2D X-ray angiography [2]. So far, multiple catheter-based invasive techniques, such as intravascular ultrasound [3], optical coherence tomography [4], intravascular magnetic resonance [5], plaque thermography [6] and angioscopy [7], have been used for the identification of unstable plaques. MDCT has emerged as a non-invasive imaging tool for plaque detection and characterization [8–17], as well as coronary artery stenosis assessment with its high negative predictive value.

The unavoidable high radiation dose is known to be a major drawback of retrospective ECG-gated coronary MDCTA. To reduce this, ECG-correlated tube current modulation (reduction of tube current in systole) is now commonly available. Prospective ECG-triggered 64-MDCTA, which can reduce radiation dose by around 80% compared to retrospective ECG-modulated 64-MDCTA, has recently been introduced [18]. In addition, to further reduce the dose, ECG-triggered 64-MDCTA with a lower tube voltage (100 kV) was applied for patients with a body mass index (BMI) of lower than 25 kg/m^2 [19,20]. Lower tube voltage has been used on CTA in various organs, as it leads to increased opacification of contrast-enhanced vascular structures owing to an increase in the photoelectric effect and a decrease in Compton scattering [21]. However, we need fundamental verification before the interpretation of CT density for prediction of plaque nature as the use of lower tube voltage alters soft tissue contrast, thereby potentially affecting the characterization of soft plaque. A previous phantom study has shown that 120 kV prospective ECG-triggered and retrospective ECG-gated 64-MDCTA were comparable in plaque imaging regarding densitometry or stenosis measurement [22]. Thus, the purpose of this study is to compare 100 kV and 120 kV prospective ECG-triggered

* Corresponding author. Tel.: +81 82 2575257; fax: +81 82 2575259.
E-mail addresses: horiguch@hiroshima-u.ac.jp (J. Horiguchi), fujioka@hiroshima-u.ac.jp (C. Fujioka), kiguchi@hiroshima-u.ac.jp (M. Kiguchi), hideyay@hiroshima-u.ac.jp (H. Yamamoto), yun.shen@ge.com (Y. Shen), ykihara@hiroshima-u.ac.jp (Y. Kihara).

0720-048X/$ – see front matter © 2009 Elsevier Ireland Ltd. All rights reserved.
doi:10.1016/j.ejrad.2009.08.002

Please cite this article in press as: Horiguchi J, et al. In vitro measurement of CT density and estimation of stenosis related to coronary soft plaque at 100 kV and 120 kV on ECG-triggered scan. Eur J Radiol (2009), doi:10.1016/j.ejrad.2009.08.002